Final Reports

Under

Contract # NAG - 5 - 1010

National Aeronautics and Space Administration

Improvement and extension of a radar forest backscattering model

Prepared by:
David S. Simonett
Yong Wang

Department of Geography
University of California Santa Barbara

October 1989

1. Introduction

Radar modeling of mangal forest stands, in the Sundarbans area of Southern Bangladesh, has been developed. The modeling employs radar system parameters such as wavelength, polarization, and incidence angle, with forest data on tree height, spacing, biomass, species combinations, and water content (including slightly conductive water) both in leaves and trunks of the mangal. For Sundri and Gewa tropical mangal forests, five model components are proposed, which are required to explain the contributions of various forest species combinations in the attenuation and scattering of mangal vegetated nonflooded or flooded surfaces. Statistical data of simulated images (HH components only) have been compared with those of SIR-B images both to refine the modeling procedures and to appropriately characterize the model output. The possibility of delineation of flooded or non-flooded boundaries is discussed.

2. Characteristics of Mangal Forests in Southern Bangladesh

2.1. Gewa and Sundri Trees

Gewa *(Excoecaria agallocha)* and Sundri *(Heritiera minor Syn. H. formes)* are mangrove species. The shoots are mostly orthotropic with infrequent diffuse branches, which sometimes may branch from the base and shrub-like form. Leaves are simple in shapes; and broad in size (Tomlinson, 1986). Gewa lacks any elaborated aerial part or pneumatophores, which function to supply oxygen to the roots at high tide. Sundri does have pneumatophores.

A mature Gewa tree grows intermittently and irregularly, up to 20 meters high for a mature tree. Branching is diffuse, irregular, and by prolepsis. The canopy is dense. *A mature Sundri tree* is about 10 to 25 meters tall, and low-branched. The branches are thick and crooked, and the canopy is very dense.

2.2. Gewa and Sundri Forest Stands

Gewa and Sundri forests occur dominantly at the tidal mouth of the Baleswar River in southern Bangladesh, which belong to closed broadleaved woody tropical rain forests (FAO, 1981). Most of the mouth areas are frequently flooded by fresh water during the monsoon rains (May - June to October - November, Chapman, 1977), with salt water intrusion during the rest of the year. Gewa and Sundri forests are very difficult of access with soft footing, and have extremely high canopy and stem densities. The mangrove forests in this area are estimated at about 590,000

hectares (FAO, 1982), which contribute very important forest resources and environmental protection for Bangladesh: they provide marketable products, and also play roles as buffers for storm surges, and tidal waves coming from the Bay of Bengal (Imhoff et al., 1986).

2.3. Ground Surfaces

The Delta soil is a clay loam lying over alternating layers of clay and sand, highly saturated with exchangeable bases (Na^+, Ca^{++}, K^+, etc.). The salinity of the soil varies seasonally as a result of the changing balance of fresh water and salt water. Chapman (1977) pointed out that there is a very high salinity at the beginning of the dry season, and this factor considerably limits the development, maintenance, or regeneration of the less halophilous species such as Sundri, which is on the way to extinction because of excessive salt water intrusion. During the rainy season (when the SIR-B images were obtained), the salinity will be low.

3. Analysis of Ground Truth Data

Ground truth data of Sundri and Gewa mangal forest in our southern Bangladesh research site were originally collected by a NASA and Bangladesh science team concurrently with the SIR-B Mission in October, 1984; and subsequently by Chaffey, et al., (1985). All these data were prepared by averaging measurements made for inventory plots (100 * 100 meters in size), consisting of:

a. a digitized forest stand map which was used to locate and extract each forest stand data from the SIR-B images. The ground surface is classified as either flooded or nonflooded surface, based on field observations.

b. DBH count distributions by DBH segments, employed to generate random aerial root (pneumatophore), and tree trunk distributions with varying DBHs in simulated stand areas.

c. tree heights and canopy depths by their DBHs were used to compute each tree height and mean canopy depth in each simulated pixel in a forest stand based on the DBH counts for each DBH segment in that pixel.

d. canopy biomass of in each DBH segment was employed to calculate attenuation coefficients of canopies.

e. gravimetric moisture content of canopies and trunks was used to derive the relative dielectric constants of the leaves and the tree trunks.

4. Radar Models of Sundri and Gewa Forest Stands

Based on the above analysis, five components are proposed, as shown in Figure 1 (see also Wang, et al., 1989):

1 Direct backscattering from various surfaces (σ^o_{dbs}),

2 volume scattering from canopy (σ^o_{vsc}),

3 double-bounce specular reflection of tree trunk-surface (σ^o_{dts}),

4 double-bounce specular reflection of aerial roots-surface (σ^o_{drs}), and

5 multiple scattering of surface-canopy (σ^o_{msc}).

Thus, the total radar return is

$$\sigma^o_{tot} = \sigma^o_{dbs} + \sigma^o_{vsc} + \sigma^o_{dts} + \sigma^o_{drs} + \sigma^o_{msc}$$

It should be noted that all these model components may or may not be attenuated by the canopy, by the aerial root layer, and/or by the tree trunk layer, depending on their presence or not (see Figure 1.).

5. Discussion

5.1. The Fit of the Models to the SIR-B Images (HH polarization only)

Three forest stands were extracted from SIR-B images (DT 120, incidence angle 26^o; and DT 104, incidence angle 46^o; see also Imhoff et al. 1986), and the image DNs were converted to relative radar backscattering coefficients (dB) by

$$\sigma^o = 10 * log\,(DN^2 - C_{1i}) - C_{2i}$$

where $i = 1, 2$, corresponding to DT 120 and DT 104. C_{1i} are the noise levels, C_{2i} constants for calibration. Both C_{1i} and C_{2i} were provided by Jet Propulsion Laboratory (JPL), as shown in Table 5.1.

The radar returns for each stand at the two incidence angles, given in Table 5.2, show that there are differences in the absolute values in that the returns from SIR-B images are lower than those of our model results. The mean (μ) and standard deviation (σ) of the differences, in dB, are μ_{26^o} = -10.9, σ_{26^o} = 0.90; and μ_{46^o} = -9.4, σ_{46^o} = 0.86. The reason for the differences may be that the models are theoretical solutions and each model component is incoherently added, which will almost certainly produce higher values than the actual coherent summation of the

electromagnetic field, which we cannot perform because of the complexity of the environment. The same evidence of higher incoherent summation was also found by Sun and Simonett (1988). Also, SIR-B had some major calibration problems, which may produce uncertainty as to the true values of C_{1i} and C_{2i} (Wall and Curlander, 1988). Because the standard deviations of the differences are relatively small, after the model results are shifted down (μ_{26^o} and μ_{46^o} for 26^o and 46^o incidence angles, respectively), the model results match the SIR-B images well in dispersion.

In order to better assess the model's ability to predict differences in returns from difference stands, stand Gn was selected as a reference, and σ^o for each stand relative to that for Gn was calculated by subtraction (equivalent to a ratio, after log10 operation). There is good agreement between the model and SIR-B results (Table 5.3): all inter-stand comparisons at both angles agreed in sign except for (SGn - Gn) and (SGn -Gn) at 26^o; and (GSn - Gn) and (SGn - Gn) at 46^o. The magnitudes of the differences agreed very well for some stands (Gf - Gn) but poorly for others (SGn - Gn, and SGf - Gn).

5.2. Radar Returns from Nonflooded and Flooded Areas

It is well understood that some types of flooded forest yield brighter L-band returns than unflooded stands (Stone and Woodwell, 1985; Richards et al., 1987). SIR-B and model results given in Table 5.4 show that although flooded stands yield higher returns than nonflooded stands in all but one case, the difference was not very great. The differences ranged from 0.5 to 3.2 dB for SIR-B images; 0.9 to 1.7 dB for model results at HH polarization; and 0.1 to 1.2 dB for model results at VV polarization. Most were less than 1.5 dB. The lack of a marked difference may result from strong attenuation by the dense canopy, and also from the uncertainty in the locations of the flooded and nonflooded areas due to changing tidal inundation, when the areas were imaged at 20:31 at GMT (3:31 am local time) for DT 120 and at 20:48 GMT (3:48 am local time) (Cimino et al., 1988). The difference in returns between flooded and nonflooded stands was, on average, greatest for GS, and least for SG, at both incidence angles. SG was the only stand for which SIR-B flooded returns were less than nonflooded returns (a 0.4 dB reduction). Due to uncertainty in calibration of σ^o, these small differences cannot be considered significant; in most cases they are less than one standard deviation of the stand means (Table 5.6). The differences are probably not large enough to delineate the flooded boundaries with confidence. Also, there are no obvious visual boundaries on the SIR-B images between those stand areas and surrounding areas, because

of the high intrinsic variance in SIR-B images and the patchiness of the flooded areas.

5.3. Differences in Radar Returns between Different Stands

For both flooded and nonflooded stands, there are only small differences (ranging -1.8 to 0.8 dB) (Table 5.5). This may be explained as follows: a) each stand is a mix of Sundri and Gewa in varying proportions; b) the number of stems is very large and the canopy is very dense, which are of importance both in enhancing σ^o_{dts} and σ^o_{drs} and in attenuation; and c) the structure of Sundri and Gewa are similar to each other (Tomlinson, 1986).

5.4. Radar Returns as a Function of Different Incidence Angles

The mean returns at different incidence angles are almost the same, but with greater variance at the smaller incidence angle, as tabulated in Table 5.6. At the smaller incidence angle, there is a shorter path length through the canopy, yielding less attenuation for the σ^o_{dts} and the σ^o_{drs} terms, which are the main component producing the variance for mangal: a similar conclusion was reached by Sun and Simonett (1988) for pine forest.

5.5. Relative Importance of Model Components

The dominant model components are σ^o_{dts} at HH polarization. At VV polarization, σ^o_{dts}, σ^o_{drs}, and σ^o_{vsc} are roughly equal to each other for nonflooded and flooded surfaces (Table 5.7). For flooded surfaces σ^o_{dts} and σ^o_{drs} are increased, and σ^o_{vsc} is unchanged. In areas where there are some natural clearings which lack the dense canopy layer, σ^o_{dts} and σ^o_{drs} are clearly dominant. The high returns from forest edges facing the radar illumination direction on the SIR-B images are notable.

6. Publication Produced under this Contract

Wang, Y., M. L. Imhoff, and D. S. Simonett, (1989), "Radar modeling of mangal forest stands", *The Proceedings of the IGARSS'89,* vol. 4, pp. 2497-2500. Vancouver, Canada, July, 1989.

Table 5.1. Conversion constants from DNs to dB for SIR-B images (HH)

	C_{1i}	C_{2i}
DT 120 (26° incidence angle)	3157.5	55.5
DT 104 (46° incidence angle)	4389.1	56.4

Formulas for conversion of SIR-B image DNs to σ^o in dBs is:

$$\sigma^o = 10 * \log[DN^2 - C_{1i}] - C_{2i}$$

where $i = 1, 2$, corresponding to DT 120 and DT 104 of SIR-B images. These data were provided Jet Propulsion Laboratory.

Table 5.2. Mean σ^o (dB) of SIR-B images (HH) and model results

Stands		Gn	Gf	GSn	GSf	SGn	SGf
26°	SIR-B images (HH)	-13.5	-12.2	-14.4	-12.2	-13.6	-14.0
	Model results (HH)	-3.1	-2.1	-3.5	-1.8	-2.5	-1.4
	Differences (HH)*	-10.4	-10.1	-10.9	-10.4	-11.1	-12.6
	Model results (VV)	-7.0	-6.8	-7.0	-6.9	-7.4	-7.0
46°	SIR-B images (HH)	-13.4	-12.1	-14.5	-11.3	-13.6	-13.1
	Model results (HH)	-4.3	-3.4	-4.0	-3.1	-3.6	-2.7
	Differences (HH)*	-9.1	-8.7	-10.5	-8.2	-10.0	-10.4
	Model results (VV)	-7.2	-6.0	-7.5	-6.3	-7.8	-6.7

* The differences are defined as the dB values of SIR-B images minus those of model results (HH). The means (μ) and the standard deviations (σ) of the differences are μ_{26^o} = -10.9, σ_{26^o} = 0.90, and μ_{46^o} = -9.9, σ_{46^o} = 0.95.

Table 5.3. Differences of (mean σ^o, in dB) for model results and SIR-B images

		Gn-Gn	Gf-Gn	GSn-Gn	GSf-Gn	SGn-Gn	SGf-Gn
26°	SIR-B images (HH)	0.0	1.3	-0.9	1.3	-0.1	-0.5
	Model results (HH)	0.0	1.0	-0.4	1.3	0.6	1.7
	Model results (VV)	0.0	0.2	0.0	0.1	-0.4	0.0
46°	SIR-B images (HH)	0.0	1.3	-1.1	2.1	-0.2	0.3
	Model results (HH)	0.0	0.9	0.3	1.2	0.7	1.6
	Model results (VV)	0.0	1.2	-0.3	0.9	-0.6	0.5

Stand Gn was selected as a reference. The radar returns for the other stands minus the return of Gn were calculated for both model results (HH and VV) and SIR-B images (HH).

Table 5.4. Differences of (mean σ^o, in dB) between flooded and nonflooded stands

		Gf - Gn	GSf - GSn	SGf - SGn
26°	SIR-B images (HH)	1.3	2.2	-0.4
	Model results (HH)	1.0	1.7	1.1
	Model results (VV)	0.2	0.1	0.4
46°	SIR-B images (HH)	1.3	3.2	0.5
	Model results (HH)	0.9	0.9	0.9
	Model results (VV)	1.2	1.2	1.1

Table 5.5. Differences of (mean σ^o , in dB) between different stands

		Nonflooded		Flooded	
		GSn - Gn	SGn - Gn	GSf - Gf	SGf - Gf
26°	SIR-B images (HH)	-0.9	-0.1	0.0	-1.8
	Model results (HH)	-0.4	0.6	0.3	0.7
	Model results (VV)	0.0	-0.4	-0.1	-0.2
46°	SIR-B images (HH)	-1.1	-0.2	0.8	-1.0
	Model results (HH)	0.3	0.7	0.3	0.7
	Model results (VV)	-0.3	-0.6	-0.3	-0.7

Gn and Gf (for model results and SIR-B images) were selected as references for nonflooded and flooded stands, respectively.

Table 5.6. σ^o (dB) as a function of incidence angles

Mean values

		Gn	Gf	GSn	GSf	SGn	SGf
SIR-B images (HH)	26°	-13.5	-12.2	-14.4	-12.2	-13.6	-13.4
	46°	-13.4	-12.1	-14.5	-11.3	-13.6	-13.1
	Differences	-0.1	-0.1	0.1	0.9	0.0	0.3
Model results (HH)	26°	-3.1	-2.1	-3.5	-1.8	-2.5	-1.4
	46°	-4.3	-3.4	-4.0	-3.1	-3.6	-2.7
	Differences	1.2	1.3	0.5	1.3	1.1	1.3
Model results (VV)	26°	-7.0	-6.8	-7.0	-6.9	-7.4	-7.0
	46°	-7.2	-6.0	-7.5	-6.3	-7.8	-6.7
	Differences	0.2	-0.8	0.5	-0.6	0.4	0.3

Standard derivations

		Gn	Gf	GSn	GSf	SGn	SGf
SIR-B images (HH)	26°	2.04	2.06	2.03	2.09	1.86	3.46
	46°	1.41	1.75	1.45	1.18	1.33	1.27
Model results (HH)	26°	0.21	0.23	0.19	0.20	0.19	0.22
	46°	0.27	0.29	0.20	0.21	0.22	0.23
Model results (VV)	26°	0.34	0.39	0.28	0.32	0.26	0.31
	46°	0.19	0.15	0.16	0.14	0.19	0.15

Table 5.7. Relative importance of model components (mean σ^o, in dB)

		σ^o_{dbs}	σ^o_{vsc}	σ^o_{dts}	σ^o_{drs}	σ^o_{msc}
-Gn	26° (HH)	-13.0	-12.7	-6.9	-8.9	-13.0
	26° (VV)	-13.4	-12.7	-16.7	-12.5	-17.0
	46° (HH)	-23.8	-13.1	-6.5	-12.9	-13.5
	46° (VV)	-20.8	-13.1	-14.7	-10.5	-21.1
Gf	26° (HH)	-22.3	-12.7	-5.3	-7.3	-11.2
	26° (VV)	-22.4	-12.7	-14.9	-10.7	-15.1
	46° (HH)	-50.3	-13.1	-5.4	-11.8	-12.2
	46° (VV)	-46.7	-13.1	-12.9	-8.7	-19.2
GSn	26° (HH)	-12.9	-12.3	-7.0	-11.5	-11.9
	26° (VV)	-12.5	-12.3	-16.2	-15.1	-15.1
	46° (HH)	-24.7	-12.7	-6.0	-13.8	-13.6
	46° (VV)	-21.9	-12.7	-14.1	-11.5	-21.3
GSf	26° (HH)	-22.9	-12.3	-4.5	-7.9	-11.0
	26° (VV)	-23.2	-12.3	-14.2	-11.4	-15.0
	46° (HH)	-51.1	-12.7	-4.9	-12.7	-12.3
	46° (VV)	-47.7	-12.7	-12.3	-9.7	-19.5
SGn	26° (HH)	-14.7	-11.9	-5.0	-10.5	-12.8
	26° (VV)	-15.3	-11.9	-15.2	-14.4	-17.0
	46° (HH)	-26.0	-12.3	-5.2	-15.1	-14.0
	46° (VV)	-23.4	-12.3	-13.4	-13.1	-21.9
SGf	26° (HH)	-23.9	-11.9	-3.5	-8.9	-11.1
	26° (VV)	-24.3	-11.9	-13.4	12.6	-15.2
	46° (HH)	-52.3	-12.3	-4.1	-14.0	-12.8
	46° (VV)	-49.3	-12.3	-11.6	-11.3	-20.1

6. References

Chaffey, D. R., F. R. Miller, and J. H. Sandom, (1985), "A forest inventory of the Sundarbans, Bangladesh", *British Overseas Development Administration Project # 140, Land Resource Development Center,* Tolworth, Surbiton, Surrey, England.

Chapman, V. J. (1977), "*Wet coastal ecosystems, Ecosystems of the world 1*", Elsevier Scientific Publication Company.

FAO, Food and Agriculture Organization of the United Nations, (1981), *Tropical resources assessment project (in the framework of the global environment monitoring system - GEMS), Forest resources of tropical Asia.*

FAO, Food and Agriculture Organization of the United Nations, (1982), *Management and utilization of mangroves in Asia and the Pacific.*

Imhoff, M. L., M. Story, C. Vermillion, F. Khan, and F. Polcyn, (1986), "Forest canopy characterization and vegetation penetration assessment with space-borne radar", *IEEE Transactions on Geoscience and Remote Sensing,* vol. GE-24, no. 4, pp. 535-542.

Cimino, J. B., B. Holt, and A. H. Richardson, (1988), "The shuttle imaging radar (SIR-B) experiment report", *JPL publication 88-2.*

Richards, J. A., P. W. Woodgate, and A. K. Skidmore, (1987), An explanation of enhanced radar backscattering from flooded forests, *International Journal of Remote Sensing,* vol. 8, pp. 1093 - 1100.

Stone, T. A. and G. M. Woodwell, (1985), "Analysis of deforestation in Amazonia using shuttle-image radar", *IEEE Cat. No. 85CH2162-6, Digest 1985 International Geoscience and Remote Sensing Symposium,* vol. II, Amherst, Ma, 574.

Sun, G. Q. and D. S. Simonett, (1988), "Simulation of L-band HH radar backscatter from coniferous forest stands: a comparison with SIR-B data", *International Journal of Remote Sensing,* vol. 9, no. 5, pp. 907 - 925.

Tomlinson, P. B., (1986), *The botany of mangroves,* Cambridge University Press.

Wall, S. D. and J. C. Curlander, (1988), "Radiometric calibration analysis of SIR-B imagery", *International Journal of Remote Sensing,* vol. 9, pp. 891 - 906.

Wang, Y., M. L. Imhoff, and D. S. Simonett, (1989), "Radar modeling of mangal forest stands", *The Proceedings of the IGARSS'89,* vol. 4, pp. 2497-2500. Vancouver, Canada, July, 1989.

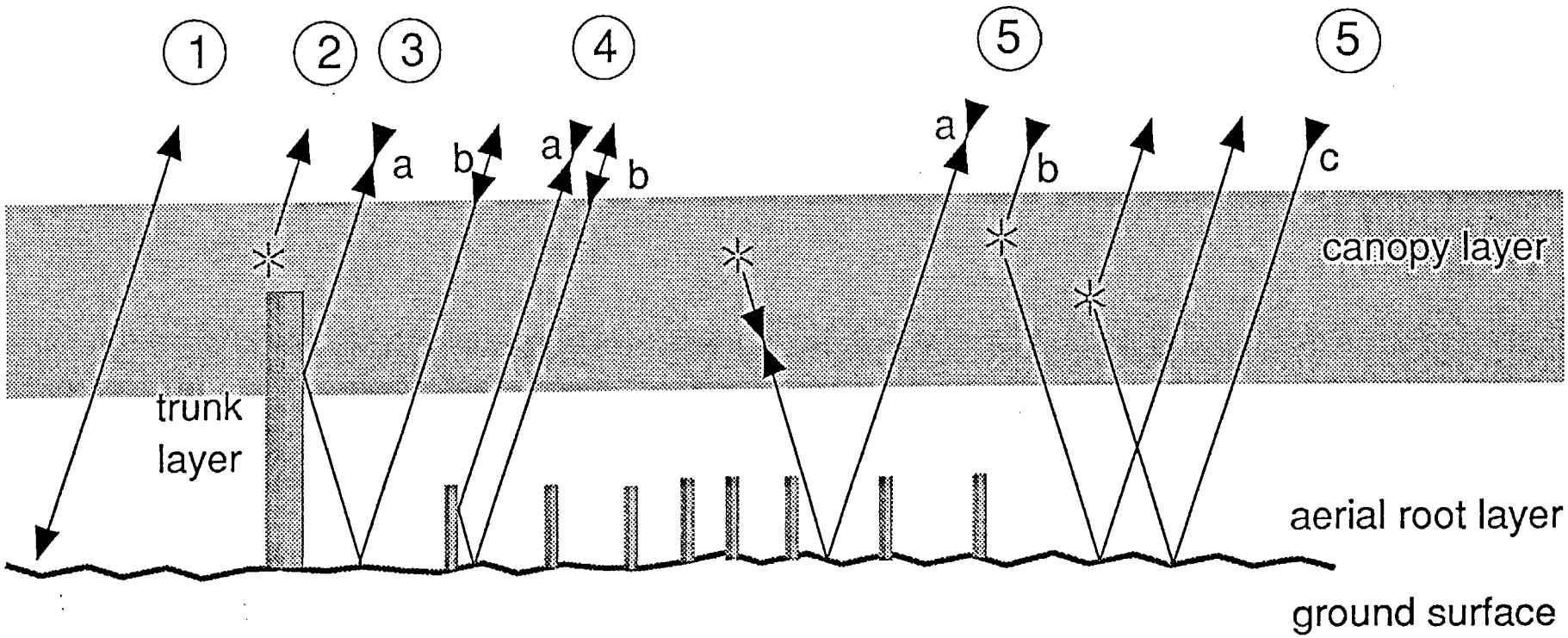

Figure 1. Model Components